International Journal of Engineering Trends and Technology
ISSN: 2231 – 5381 /doi:10.14445/22315381/IJETT-V69I10P221
Volume 69 Issue 10, 168-177, October, 2021

Seismic Performance Limit States Assessment of Bridge Piers by Numerical Analysis and Experimental Damage Observations

Mohamed Saad Abbadi[1], Nouzha Lamdouar[2]

[1]*Civil Engineering Laboratory, Mohammadia School of Engineers, Mohammed V University in Rabat, Morocco*

[1]saadabbadi@research.emi.ac.ma, [2] lamdouar@emi.ac.ma

Abstract. - *A numerical model of the bridge piers is achieved through the OpenSees program in order to predict the nonlinear global and local responses, expressed as displacements, forces and strains. The model is first evaluated by comparing the numerical force-displacement response with the corresponding experimental force-displacement response for different degrees of damages. Also, the limit states are compared to see how accurately the model predicts the local behavior as well. Experimental results of 39 columns tested under cyclic loading by several authors are used. These columns cover the main parameters of interest for typical bridge piers, such as geometry, longitudinal and transverse reinforcement ratio, and axial loading ratio. The results of this comparison have led to the conclusion that the numerical model can accurately predict the observed damage sequence and, therefore, the limit states that will be used to achieve the performance objectives. Safety coefficients are proposed to cover the error between the numerical model and experimental responses.*

Keywords — *Performance objectives, OpenSees, Pushover analysis.*

I. INTRODUCTION

Performance-based seismic design is based on the approach that guarantees criteria for the functionality and durability of existing structures. These criteria, called performance limit states, are usually defined qualitatively in terms of the damage state of the structure. However, the quantitative definition of these qualitative damage limit states must be made in relation to reference values that accurately reflect the qualitative states such as strain, displacement, and curvature. Material strain values, such as the compressive strain of concrete and tensile strain of steel, are inherent material properties that can be related to the limit states and have been commonly used in the literature.

Several authors have addressed the issue of qualitatively defining the performance limit states of bridge piers. For example, the Oregon Department has identified two limit states that are strain-based and accordingly provided concrete tensile strain values for these two levels of limit states. In addition, Goodnight and Kowalsky (2015) experimentally evaluated the deformation limits of reinforced concrete column performance through 30 specimens. As a result, they propose relative strain values for the concrete and reinforcing steel for limit states. These values are in agreement with the results provided by Kowalsky (2000). Hose & Seible (1999) suggest five levels of performance and propose quantitative values corresponding to them. These values are based primarily on observations of damage to the tested pier specimens during the damage sequence from minor deformation and early cracking to reinforcement buckling. Transportation Research Board also provides reinforcement and concrete deformation values for five limit states.

Kowalsky et al. 1996 carried out a series of three tests on columns subjected to hysteretic stresses. The observation was made on the appearance of cracks in the cover concrete subjected to compressive stresses. The compressive strains at the extreme fiber level are 0.0025, 0.003, and 0.0036, respectively. Kunnath et al. 1997 developed an experimental program to illustrate the progressive damage of bridge columns and identify criteria to describe this damage sequence, and correlate visual observations to damage limit states. For this purpose, 12 specimens were recommended and subjected to different types of loading (monotonic, hysteretic, accelerograms,...). The initiation of cracking is observed from a tensile strain of 0.002 to 0.004 for the test n°1. For the other tests, the magnitude of the seismic load does not allow the identification of light damage. Lehman et al. 1998 conducted an experimental campaign and identified 4 limit states. Each limit state is associated with a degree of observed damage. These observations are cracking, plasticization of the longitudinal reinforcement, spalling of the cover concrete, and failure of the transverse reinforcement.

This study focused on defining a link between the qualitative criteria expressed in terms of observed damage and the reference values that characterize them. For this purpose, the results of several experimental campaigns carried out on columns have been used to calibrate and validate the numerical modeling of these columns.

II. MATERIALS AND METHODS

This section describes first the damage sequence observed on cyclic tests and proposes strain limits that suit the most to these damage states. Then, an overview of the numerical modeling strategy is presented, with the description of the necessary steps to obtain the best number of fibers, integration points, and material properties.

A. Experimental damage sequence

The first damage observed is cracking. The limitation of cracks allows keeping bridge piers in the elastic behavior. This limit state corresponds to a fully elastic state of the structure after a seismic event. The tensile strain of the extreme fiber of the pier is used to express this limit state, and the recommended value varies from 0.0005 to 0.001. In addition, in order to evaluate the concordance of this value with observations made on piles subject to cyclic loadings, several simulations of the tensile deformation of the extreme fiber were performed and compared with the experimental results. The best value obtained was 0.001.

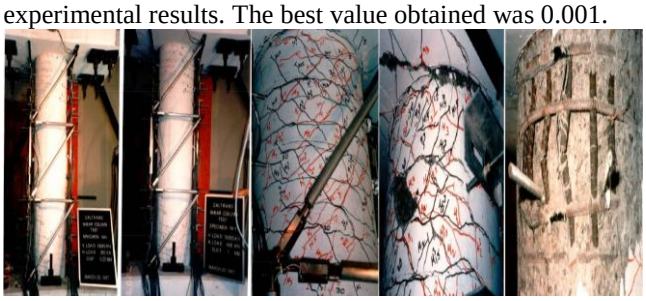

Fig 1. Damage sequence of columns, from light cracking to buckling

Then, the yielding of longitudinal reinforcements occurs. This limit state is linked to the beginning of yielding of the longitudinal reinforcement located at the most tensed end of the pile and expresses the appearance of the first damages of the structure resulting in residual displacements that need to be repaired after the seismic event. It is expressed by the value of strain of 0.02 of the longitudinal steels.

Thereafter, it's noticed the onset of spalling of cover concrete. This limit state corresponds to a state of moderate damage of the structure, which is manifested by the loss of the coverage of the longitudinal and transverse steels, and which requires important post-seismic repair interventions.

This limit state is quantified by the compression deformation of the extreme fiber of the concrete cover at -0.04.

In the end, buckling occurs in longitudinal reinforcement.

This limit state is associated with the failure of the stirrups that confine the longitudinal reinforcements. This failure occurs at the compressive strain of the longitudinal reinforcements corresponding to the state of this failure and determined according to the energy balance model proposed by [Mander et al.]

This deformation depends on several parameters mainly related to the mechanical characteristics of the steel and concrete constituting the pile as well as the spacing of the transverse reinforcements.

The following table summarizes these different limit states:

TABLE I: Strains corresponding to Damage observations

Damage observation	Corresponding strain
Crack prevention	0.001
Yielding of longitudinal reinforcement	0.02
Spalling of cover concrete	-0.04
Buckling of longitudinal reinforcement	ε_{cu}

B. Numerical model

In order to carry out numerical modeling allowing to represent faithfully the degree of damage undergone by the columns under seismic solicitations, the specimens having been used for the experimental tests summarized in the table below are reproduced numerically. Thus, a pushover analysis on a distributed plasticity model in OpenSees is conducted. The model considers the whole element having non-linear properties, and the inelasticity is expressed at the specified predefined cross-sections, commonly called integration points. Each cross-section is divided into several fibers, and each of these fibers is governed by its own stress-strain relationship that reflects the constitutive material (unconfined concrete, confined concrete, longitudinal steel). The global non-linearity of the columns is obtained by integrating the contribution of each section, which allows reaching a higher level of accuracy compared to methods that concentrate the plasticity at the regions where plastic hinges occur.

The materials constituting the piles are steel, confined concrete, and cover concrete. Mander's model is used to describe the behavior of confined concrete, while the bilinear model with strain hardening is used to describe steel.

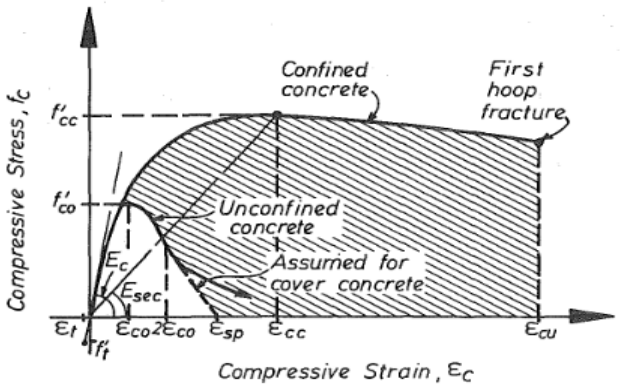

Fig 2. Stress-strain model of confined concrete

A necessary step is to perform a convergence study, allowing to define of the number of fibers and integration points to be recommended, as well as the stress-strain model of the materials constituting the columns. The objective of this convergence study is to reduce as much as possible the relative error between the characteristic indicators obtained by tests and those obtained by the corresponding numerical models. Those indicators are the displacements at top columns, base shear, concrete and steel strains along the damage sequence of the columns (concrete cracking, buckling of the reinforcement, failure of the stirrups,..). Thus, due to the large number of

parameters involved in this study, the convergence is carried out in 3 phases described as follow:

Phase 1 of the convergence study

The column cross-sections were discretized into small fibers in which each fiber has a defined uniaxial stress-strain relationship. The cross-section is discretized using a radial scheme with Ncr core concrete divisions, Ntc covers concrete core divisions and Nru concrete divisions in the transverse direction. The concrete core, cover concrete, and longitudinal steel fibers are associated with a uniaxial stress-strain model corresponding to the material they represent.

In order to define the optimal number of fibers to recommend, a moment-curvature analysis is performed for different mesh arrangements summarized in the following table:

TABLE II: **Mesh arrangements adopted**

Simulation	Nru	Ncr	Ntc
1	8	8	8
2	12	12	12
3	16	16	16
4	20	20	20
5	24	24	24
6	28	28	28
7	32	32	32
8	36	36	36
9	40	40	40

The optimal mesh is the one that minimizes the relative error in terms of the moment-curvature. Those errors are expressed as follows:

$$Error(i) = \frac{(A^{i+1}_{Moment\_curvature} - A^{i}_{Moment\_curvature})}{A^{i}_{Moment\_curvature}}$$

Phase 2 of the convergence study

Phase 2 of the convergence study focuses on the optimal number of integration points to best reflect the flexural behavior of the columns. In order to define the optimal number of integration points to recommend, a force-displacement analysis is performed for different numbers of integration points.

TABLE III: **number of integration points adopted**

Simulation	Npi
1	3
2	4
3	5
4	6
5	7
6	8

The optimal mesh is the one that minimizes the relative error in terms of forces and displacements, and this error is expressed as follows:

$$Error(i) = \frac{(A^{i+1}_{Force\_Displacement} - A^{i}_{Force\_Displacement})}{A^{i}_{Force\_Displacement}}$$

Strain compression of cover concrete at extreme fiber and maximum tensile strain of extreme longitudinal steel is also taken as indicators of column performance. Thus the corresponding errors are expressed as follow:

$$Error(i) = \frac{(A^{i+1}_{Concrete\_Stress\_strain} - A^{i}_{Concrete\_Stress\_strain})}{A^{i}_{Concrete\_Stress\_strain}}$$

$$Error(i) = \frac{(A^{i+1}_{Steel\_Stress\_strain} - A^{i}_{Steel\_Stress\_strain})}{A^{i}_{Steel\_Stress\_strain}}$$

The chosen strains are the indicators of the degree of cracking, spalling, and yielding and thus are important parameters in the description of the damage sequence.

Phase 3 of the convergence study

Phase 3 of the convergence study is the most important step, as it is concerned with minimizing the difference between the results of the corresponding experimental and numerical tests. The parameters that allow minimizing the error are the Initial stiffness of concrete and the hardening ratio of the reinforcing steel.

To evaluate the capability of the model, the experimental results of 39 columns tested under cyclic loading by multiple authors are used. These eight columns cover the main parameters of interest for typical bridge piers. In addition, such data is available on these experimental tests. These data include:

- The force and displacement history;
- The damage observation;
- Strain gauge history;

The main properties of these columns are summarized below:

TABLE IV: **Properties of test columns**

Authors	Number of tests	Diameter column	height	Diameter longitudinal reinforcement	Number longitudinal bars	Diameter transversal reinforcement	Hoop spacing	Cover	Axial load	Concrete strength	Long steel strength	Trans steel strength
Kowalsky	1	457	3656	15.9	30	9.5	76	30.2	1780	36.6	477	445
	2	457	3656	15.9	30	6.4	51	30.2	1780	40	477	437
	33	457	3656	15.9	30	9.5	76	30.2	1780	38.6	477	445
Kunnath	1	305	1372	9.5	21	4	19	14.5	200	29	448	434

	2	305	1372	9.5	21	4	19	14.5	200	29	448	434
	3	305	1372	9.5	21	4	19	14.5	222	35.5	448	434
	4	305	1372	9.5	21	4	19	14.5	222	35.5	448	434
	5	305	1372	9.5	21	4	19	14.5	222	35.5	448	434
	6	305	1372	9.5	21	4	19	14.5	222	32.8	448	434
	7	305	1372	9.5	21	4	19	14.5	222	32.8	448	434
	8	305	1372	9.5	21	4	19	14.5	222	32.5	448	434
	9	305	1372	9.5	21	4	19	14.5	200	27	448	434
	10	305	1372	9.5	21	4	19	14.5	200	27	448	434
	11	305	1372	9.5	21	4	19	14.5	200	27	448	434
Lehman	415	609.6	2438.4	15.9	22	6.4	31.8	22.2	653.86	31	462	606.8
	815	609.6	4876.8	15.9	22	6.4	31.8	22.2	653.86	31	462	606.8
	1015	609.6	6096	15.9	22	6.4	31.8	22.2	653.86	31	462	606.8
	430	609.6	2438.4	15.9	44	6.4	31.8	22.2	653.86	31	462	606.8
NIST	1	250	750	7	25	3.1	9	9.9	120	24.1	446	441
	2	250	750	7	25	3.1	9	9.9	239	23.1	446	441
	3	250	1500	7	25	2.7	14	9.7	120	25.4	446	476
	4	250	750	7	25	3.1	9	9.9	120	24.4	446	441
	5	250	750	7	25	3.1	9	9.9	239	24.3	446	441
	6	250	1500	7	25	2.7	14	9.7	120	23.3	446	476
Wong	1	400	800	16	20	10	60	20	907	38	423	300
	2	400	800	16	20	6	65	18	1813	37	475	340
	3	400	800	16	20	10	60	20	1813	37	475	300
Soesianawati	1	400	1600	16	12	7	85	13	744	46.5	446	364
	2	400	1600	16	12	7	85	13	744	46.5	446	364
	3	400	1600	16	12	7	91	13	2112	44	446	364

	4	400	1600	16	12	7	94	13	1920	40	446	255
Tanaka	1	400	1600	20	8	12	80	40	819	25.6	474	333
	2	400	1600	20	8	12	80	40	819	25.6	474	333
	3	400	1600	20	8	12	80	40	819	25.6	474	333
	4	400	1600	20	8	12	80	40	819	25.6	474	333
	5	550	1650	20	12	12	110	40	968	32	511	325
	6	550	1650	20	12	12	110	40	968	32	511	325
	7	550	1650	20	12	12	90	40	2913	32.1	511	325
	8	550	1650	20	12	12	90	40	2913	32.1	511	325

The first aspect of the numerical model to be evaluated is the ability of the model to predict the overall behavior of the column. Therefore, the individual piles were modeled and subjected to incremental progressive displacement. The numerical force-strain responses of the 39 tests are presented in Figure 3 to Figure 12.

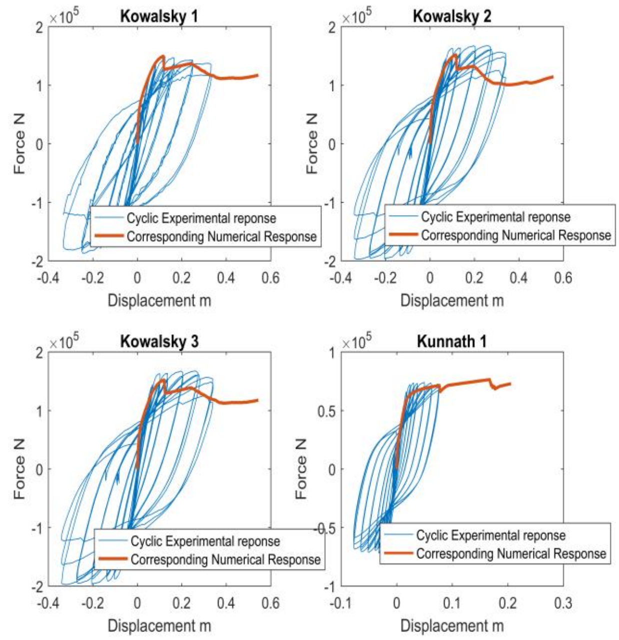

Fig 3. Force displacement Responses of tests 1 to 4

It can be noticed that the force-displacement behavior of all columns is very well predicted. Indeed, the numerical and experimental curves are practically juxtaposed to each other.

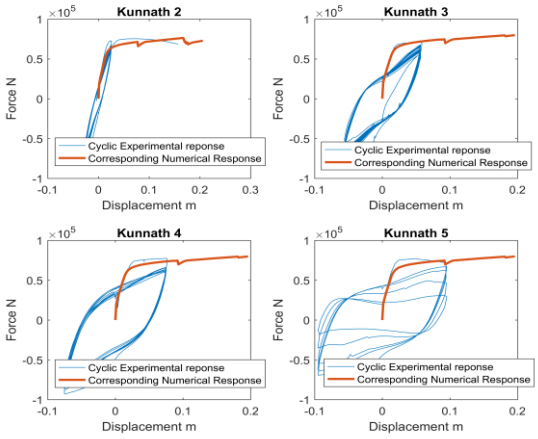

Fig 4. Force displacement Responses of tests 5 to 8

The second aspect evaluated is the local behavior. The damage levels prescribed are the concrete cracking, yielding of longitudinal reinforcement, loss of concrete cover, and finally buckling of longitudinal reinforcement.

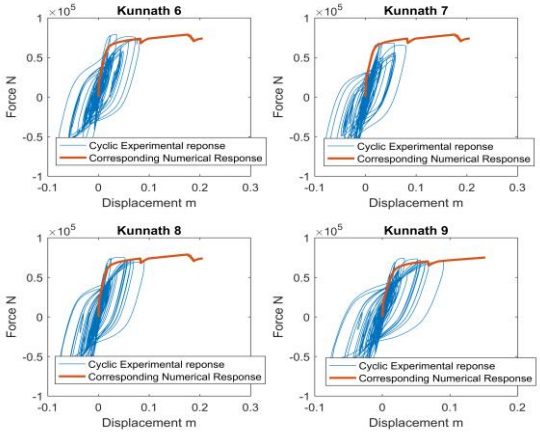

Fig 5. Force displacement Responses of tests 9 to 12

Concrete cracking is examined since it represents the first state of damage and establishes the boundary between the fully operational and operational performance levels.

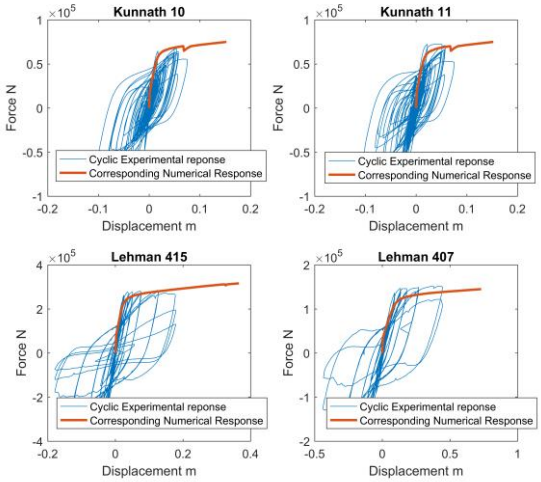

Fig 6. Force displacement Responses of tests 13 to 16

Representing the boundary between operational and delayed operational performance, the yielding of longitudinal reinforcement is also considered in the evaluation of the numerical model's ability to properly predict column behavior.

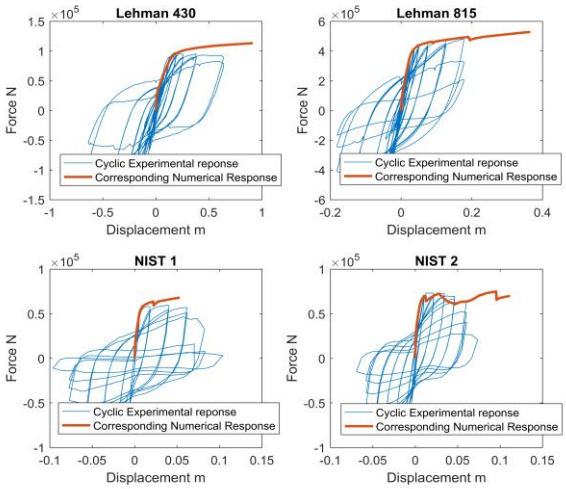

Fig 7. Force displacement Responses of tests 17 to 20

The loss of concrete cover is also considered in the evaluation of the local behavior since this limit state defines the level of delayed operation performance.

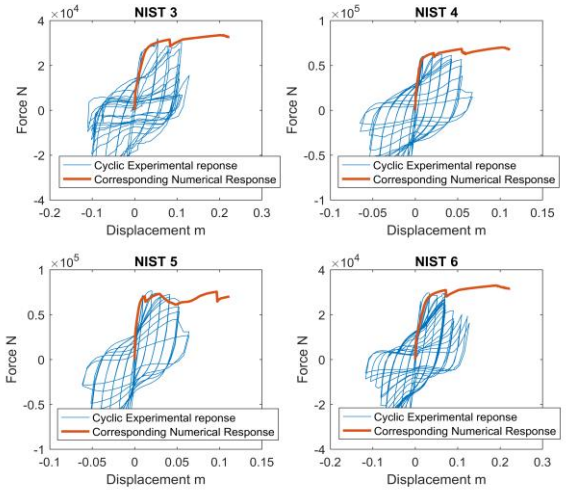

Fig 8. Force displacement Responses of tests 21 to 24

Finally, buckling of longitudinal reinforcement is the last local limit state evaluated and defines the level of near-collapse performance, where significant residual displacements are noticed, and major repair operations are needed.

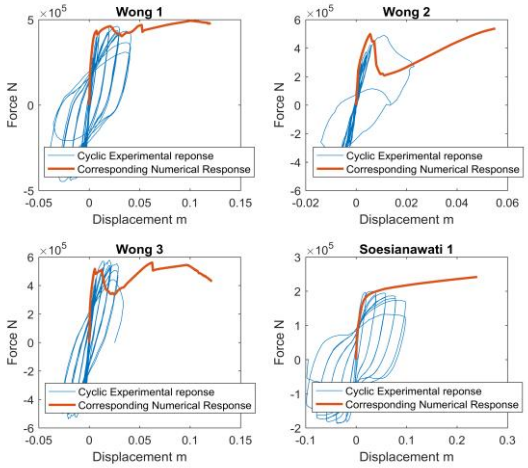

Fig 9. Force displacement Responses of tests 25 to 29

A set of simulations are conducted with different values of strain hardening of steel and initial stiffness of concrete. Initial stiffness is expressed as a multiple of young modulus, where hardening is expressed as a percentage of initial young modulus.

The values are summarized below:

TABLE V: Values of Hardening and Initial Stiffness

simulation	Hardening ratio	Initial stiffness
1	0	Ec
2	1	1.5Ec
3	2	2Ec
4	3	2.5Ec
5	4	3Ec

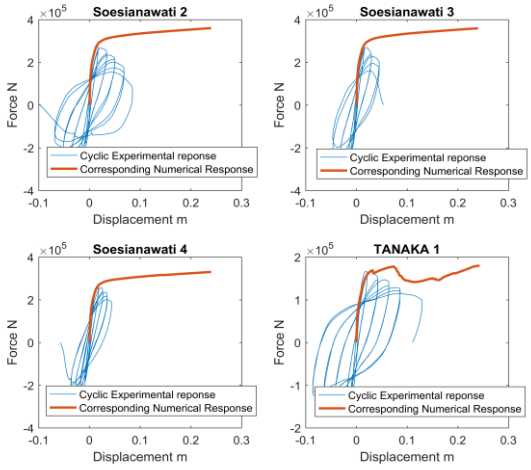

Fig 10. Force displacement Responses of tests 30 to 34

The optimal hardening ratio and initial stiffness are the parameters that minimize the relative difference of force-displacement curves and the differences in terms of damage limit states.

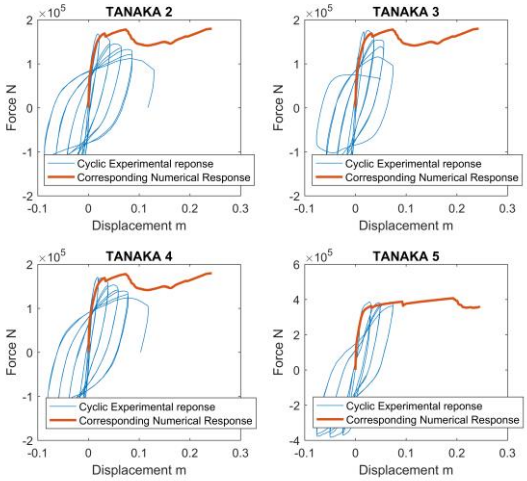

Fig 11. Force displacement Responses of tests 35 to 34

The values of Ec for the Initial stiffness of concrete and 1% for the strain hardening ratio of steel are adopted since they provide the best results.

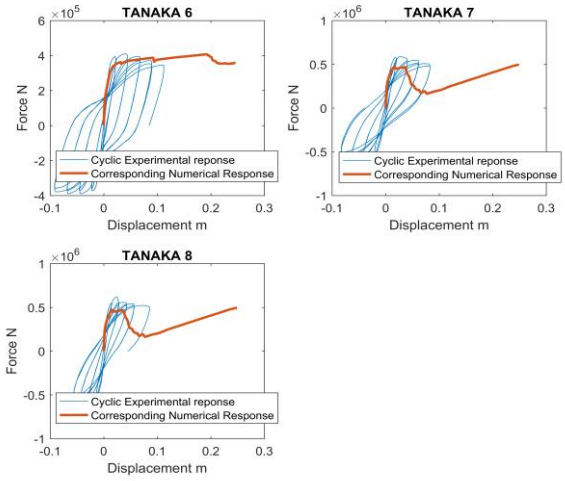

Fig 12. Force displacement Responses of tests 35 to 39

III. RESULTS AND DISCUSSIONS

The results of the 3 phases described above are presented in this section.

The first result corresponds to the relative error of the curvature response of the 39 columns described above for two successive mesh arrangements. This error begins to be stable from a mesh arrangement of 32 divisions. Thus this mesh will be adopted for the rest of the study.

The comparison between the experimental results and the results of the numerical model makes it possible to conclude that the numerical representation carried out is in agreement with the real observations of the damage. In addition, the following graphs summarize the percentages of errors obtained for the various limit states.

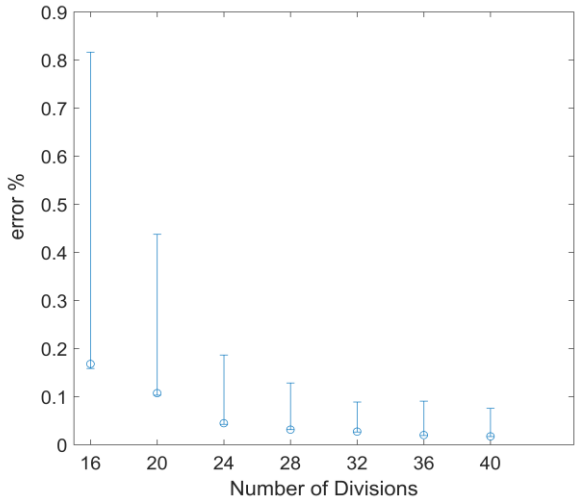

Fig 13. Relative error of displacement for the 39 columns and their average for different mesh arrangements

The optimal number of integration points is defined by minimizing the relative error of the progressive displacement between two successive numbers of points, as well as the strains at the extreme fibers in compression of concrete and tension of steel.

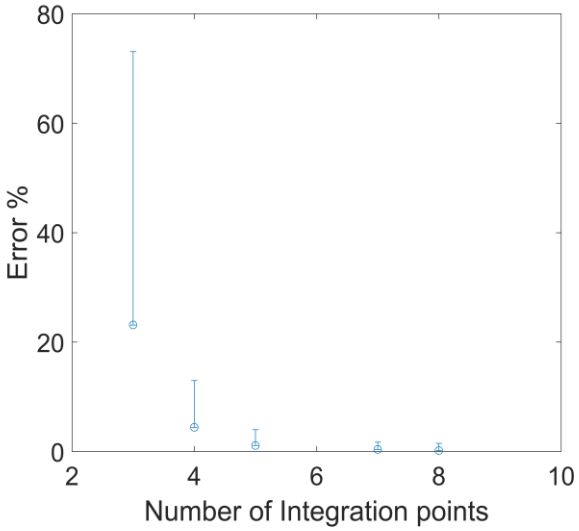

Fig 14. Relative error of displacement for the 39 columns and their average for different numbers of integration points

From the figures representing the relative errors of the 39 columns as well as their average, it is thus noted that the error stabilizes from 8 points of integration, and this is for the 3 recommended indicators prescribed above.

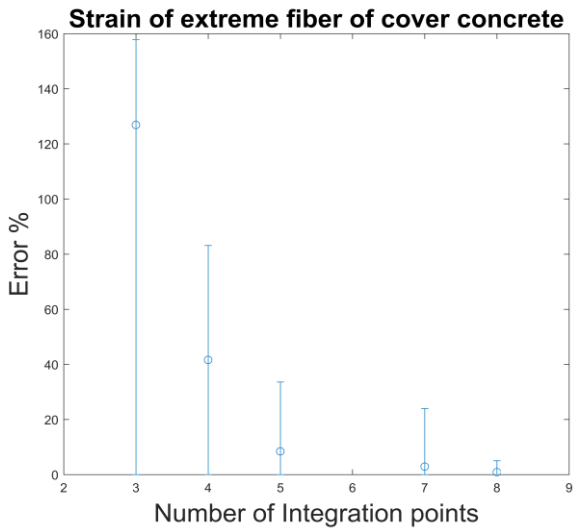

Fig 15. Relative error of cover concrete strain for the 39 columns and their average, for different number of integration points

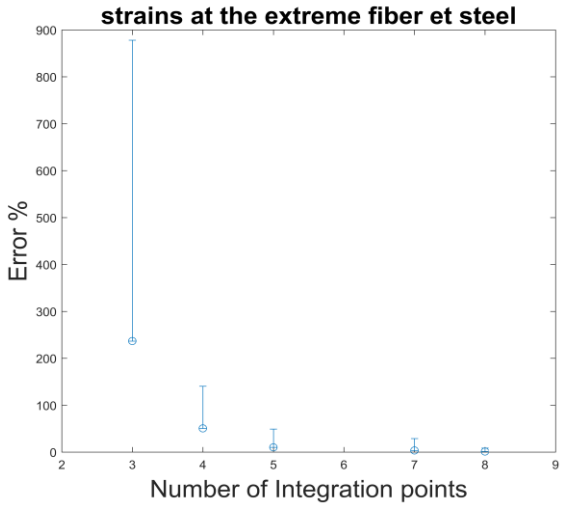

Fig 16. Relative error of steel strain for the 39 columns and their average, for different number of integration points

In the phase 3, in the first instance, the global behaviour of the numerical model of the 39 columns is compared to the corresponding experimental results through the force-displacement curves.

This comparison is made for several displacement increments in order to appreciate the difference of the two curves for different degrees of damage states.

The results of this comparison are summarized in the following figure.

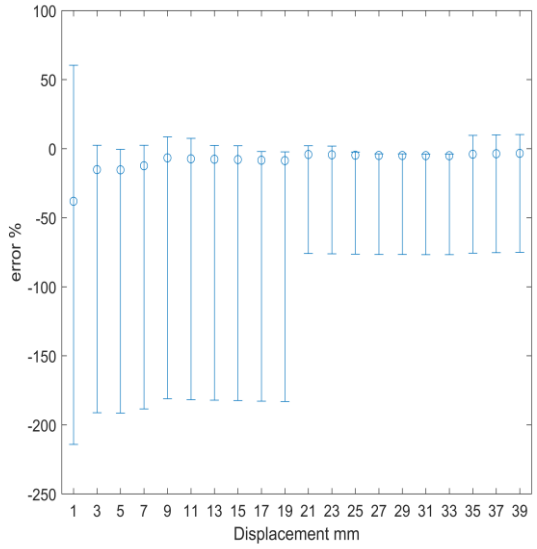

Fig 17. Error between the force displacement curve of the numerical model and the corresponding experimental results, for multiple degrees of damage.

This figure represents the results of the 39 columns and their average, and indicates the minimum, maximum and average errors obtained.

The errors vary considerably between columns for small displacements, which can be up to 200% and for an average between columns of almost 50%. This is mainly due to the fact that the observations made for the early limit states and especially those related to the cracking of the concrete cover, vary between the authors and depends on the appreciation of each of them.

This error decreases for larger displacements. It stabilizes around 70% and the average error is around 0%.

On second instance, the points that represent the limit states defined above, and from the numerical models and experimental results are compared.

These points represent successively cracking of the cover concrete, yielding of the longitudinal reinforcements, spalling of the cover concrete and finally buckling of the longitudinal reinforcements

The following table summarizes the differences between the limit points obtained from numerical models and those obtained from experimental results.

TABLE VI: Differences on % between numerical and experimental results

		Cracking		Yielding		Spalling		Buckling	
Kowalsky	1	-	-	-	-	-	-	-	-
	2	-	-	-	-	-	-	-	-
	3	-	-	-	-	-	-	-	-
Kunnath	1	-8.5	32	16	-4	13	-6.7	-12	-8
	2	-	-	16	-7	-	-	-12	-8.9
	3	-8.5	85	9.7	0.4	-	-	-12	-1.1
	4	-8.5	70	9.7	-0.8	-	-	-12	-7.7
	5	-8.5	350	9.7	-8.6	-	-	-12	-8.2
	6	-	-	16	-13	-	-	-12	-7.5
	7	-8.5	269	16	-0.7	-	-	-12	2.9
	8	-8.5	42	16	-9.7	-	-	-12	-6.5
	9	-8.5	28	16	-10	-	-	-9.4	-7.1
	10	-8.5	91	16	3.1	-	-	-9.4	2
	11	-8.5	130	16	-12	-	-	-9.4	-5.8
Lehman	415	-2.4	8.8	-	-	46	12	-	-
	815	-2.4	19	-	-	-	-	-	-
	1015	-8.5	7.2	-	-	-	-	-	-
	430	-2.4	21	-	-	-12	-1	-	-
NIST	1	-	-	-10	3.9	-4	8.1	-	-
	2	-	-	-	-	-25	-9.8	5	-9.4
	3	-	-	2.8	0.9	-10	3.2	-	-
	4	-	-	-10	-4.5	-4	1.4	-10	-1.4
	5	-	-	-	-	0	-10	-21	-12
	6	-	-	2.8	-3.6	-19	84	-	-
Wong	1	-20	47	12	68	-12	1.6	-28	5.8
	2	-20	44	12	27	-36	-5.5	12	28
	3	-20	76	12	31	-28	-4.6	44	24
Soesianawati	1	6.6	34	-4	-7.8	10	23	284	9.5
	2	6.6	58	-4	12	44	71	-1	45
	3	6.6	40	-4	8.8	44	1000	-1	965
	4	6.6	38	-4	9.3	12	53	-1	51
Tanaka	1	-	-	28	-1.2	0	4.7	-20	14
	2	-	-	28	-1.9	17	0.5	-60	53
	3	-	-	28	-0.9	17	-2.4	0	8
	4	-	-	28	-0.9	25	-1.8	0	11
	5	-	-	21	-2.1	-21	-5.6	-17	-7
	6	-	-	-9.2	-12	13	-9.3	23	-9
	7	-	-	-17	-18	-26	-23	15	-20
	8	-	-	10	-10	-14	-26	-23	-17

These results are represented by histograms as well as the lognormal function that best matches the distributions obtained.

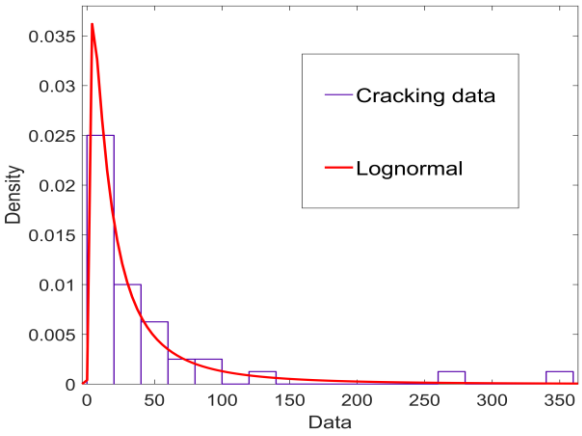

Fig 18. Distributions of difference percentage between numerical and experimental displacements corresponding to the cracking limit state.

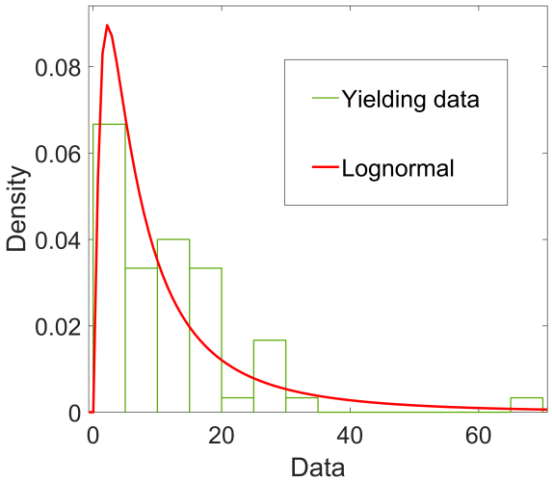

Fig 19. Distributions of difference percentage between numerical and experimental displacements corresponding to the yielding limit state.

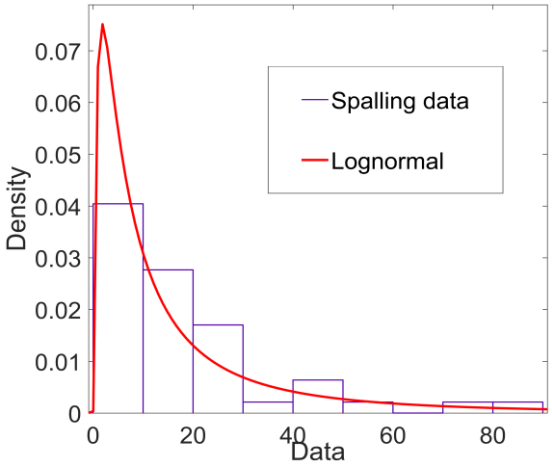

Fig 20. Distributions of difference percentage between numerical and experimental displacements corresponding to the spalling limit state.

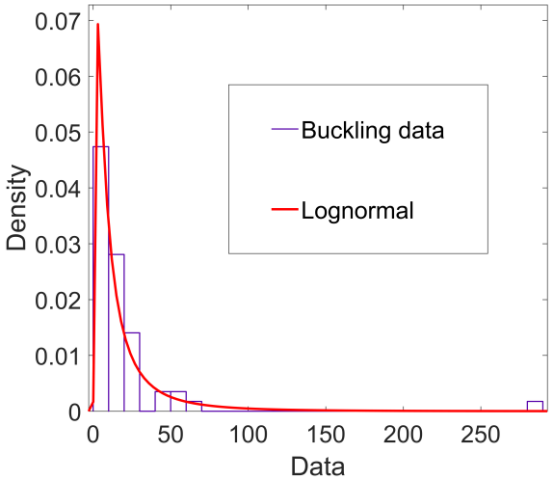

Fig 21. Distributions of difference percentage between numerical and experimental displacements corresponding to the buckling limit state.

The statistical results are summarized in the table below.

TABLE VII: Mean, Variance and 95% confidence interval of the limit state differences

	Mean	Variance	95% confidence interval	Partial coefficient
Cracking	39	5400	144	2.44
Yielding	13	416	49	1.49
Spalling	21	2038	81	1.81
Buckling	19	1190	70	1.70

IV. CONCLUSIONS

In conclusion, the results of the comparison between numerical and experimental results clearly show that the numerical model allows describing the damage sequence obtained during the cyclic tests on column specimens. However, and in order to take into account the differences observed, partial coefficients are proposed to compensate for these differences and are calculated from the deviations at 95% confidence interval.

REFERENCES

[1] F. F. Taucer, E. Spacone, and F. C. Filippou, A Fiber Beam-Column Element For Seismic Response Analysis Of Reinforced Concrete Structures, 141.

[2] S. Popovics, A numerical approach to the complete stress-strain curve of concrete, Cement and Concrete Research, 3(5) (1973) 583–599, doi: 10.1016/0008-8846(73)90096-3.

[3] K. Porter, R. Kennedy, and R. Bachman, Creating Fragility Functions for Performance-Based Earthquake Engineering, Earthquake Spectra, 23(2) (2007) 471–489, doi: 10.1193/1.2720892.

[4] S. K. Kunnath, A. El-Bahy, A. W. Taylor, and W. C. Stone, Cumulative seismic damage of reinforced concrete bridge piers, National Institute of Standards and Technology, Gaithersburg, MD, NIST IR 6075, 1997. doi: 10.6028/NIST.IR.6075.

[5] M. J. Kowalsky, Deformation Limit States for Circular Reinforced Concrete Bridge Columns, J. Struct. Eng., 126(8) (2000) 869–878, doi: 10.1061/(ASCE)0733-9445(2000)126:8(869).

[6] J. C. Goodnight, M. J. Kowalsky, and J. M. Nau, Effect of Load History on Performance Limit States of Circular Bridge Columns, J. Bridge Eng., 18(12) (2013) 1383–1396, doi: 10.1061/(ASCE)BE.1943-5592.0000495.

[7] D. Lehman, J. Moehle, S. Mahin, A. Calderone, and L. Henry, Experimental Evaluation of the Seismic Performance of Reinforced Concrete Bridge Columns, J. Struct. Eng., 130(6) (2004) 869–879, doi: 10.1061/(ASCE)0733-9445(2004)130:6(869).

[8] K. R. Mackie and B. Stojadinovi, Fragility Basis for California Highway Overpass Bridge Seismic Decision Making, 239.

[9] Guidelines-for-Performance-Based-Seismic-Bridge-Design-NCHRP-12-106-Tom-Murphy.pdf.

[10] M. Shinozuka, M. Q. Feng, H.-K. Kim, and S.-H. Kim, Nonlinear Static Procedure for Fragility Curve Development, J. Eng. Mech., 126(12) (2000) 1287–1295, doi: 10.1061/(ASCE)0733-9399(2000)126:12(1287).

[11] Y. D. Hose and F. Seible, Performance Evaluation Database for Concrete Bridge Components and Systems under Simulated Seismic Loads, 113.

[12] M. P. Berry and M. O. Eberhard, Performance Modeling Strategies for Modern Reinforced Concrete Bridge Columns, 210.

[13] A. Floren and J. Mohammadi, Performance-Based Design Approach in Seismic Analysis of Bridges, J. Bridge Eng., 6(1) (2001) 37–45, doi: 10.1061/(ASCE)1084-0702(2001)6:1(37).

[14] H. Tanaka and R. Park, Prediction of the ultimate longitudinal compressive concrete strain at hoop fracture using energy considerations, BNZSEE, 20(4) (1987) 290–305, doi: 10.5459/bnzsee.20.4.290-305.

[15] M. N. Sheikh and F. Legeron, Seismic performance-based design of bridges with quantitative local performance criteria, 11.

[16] Shear and Flexural Behavior of Lightweight Concrete Bridge Columns in Seismic Regions, SJ, 96(1) (1999), doi: 10.14359/605.

[17] Y. L. Wong, Squat circular bridge piers under multi-directional seismic attack, 277.

[18] J. C. Goodnight, M. J. Kowalsky, and J. M. Nau, Strain Limit States for Circular RC Bridge Columns, Earthquake Spectra, 32(3) (2016) 1627–1652, doi: 10.1193/030315EQS036M.